31st Annual International Conference of the IEEE EMBS
Minneapolis, Minnesota, USA, September 2-6, 2009

Model Based Reconstruction for Simultaneously Imaging Cerebral Blood Flow and De-oxygen Hemoglobin Distribution

Peng Miao, *Student Member, IEEE,* Nan Li, *Student Member, IEEE,* Abhishek Rege, Shanbao Tong, *Member, IEEE,* and Nitish Thakor *Fellow, IEEE*

***Abstract*— Laser speckle imaging (LSI) and optical intrinsic signal (OIS) imaging are shown to produce high resolution information of cerebral blood flow(CBF) and de-oxygen hemoglobin(dHb) respectively. However, the cortex curvature and non-uniform illumination always result in the inhomogeneous impact and thus distort the CBF and dHb results. In this paper, we propose to extract both CBF and dHb images from raw speckle images. A parametric model for such inhomogeneity is estimated by adaptive window median-mean filtering and curve fitting technique to reconstruct the CBF and dHb image.**

I. INTRODUCTION

As a two-dimensional optical imaging technique with high spatiotemporal resolution, laser speckle imaging (LSI) technique [1] has been widely used in studying the cerebral blood flow (CBF) [2] based on the scattering property of blood cells. In most literatures, two typical wavelengths (635 nm [3] and 780 nm [2]) have been used.

Optical intrinsic signal (OIS) [4] imaging is a neuroimaging technique based on light absorption property of cortical tissue. In the rat's cortex, the absorption of 635 nm laser is predominantly determined by the concentration of de-oxygen hemoglobin (dHb). So the area with higher dHb concentration, like the venules, implies stronger absorption and thus results in darker cortical image.

Technically, simultaneously imaging CBF and dHb distribution is feasible with 635nm laser. Ideally, when coherent 635 nm laser *uniformly* illuminates a *flat* tissue surface with moving scattering particles, such as blood cells, the 'raw speckle images' from the CCD camera contain the information of both CBF and dHb. On the one hand, speckle contrast K defined as the temporal standard derivation σ_t to the mean intensity $\langle I \rangle$ is related to the velocity v (Eq.1) (LASCA [5]); on the other hand, the mean intensity $\langle I \rangle$ which eliminates the scattering effect with improved signal noise ratio, is determined by the concentration of dHb level C [6]. By analyzing speckle contrast (LSI) and mean intensity (OIS) in each pixel over a time period, we can obtain CBF and dHb images over the cortex respectively.

$$K^2 = (\frac{\sigma_t}{\langle I \rangle})^2 \propto \frac{1}{v} \tag{1}$$

P. Miao and S. Tong are with Med-X Research Institute, Shanghai Jiao Tong University, 1954 Huashan Road, Shanghai 200030, China shanbao.tong@gmail.com

N. Li, A. Rege and N. Thakor are with the Department of Biomedical Engineering, Johns Hopkins University School of Medicine, 720 Rutland Avenue, Baltimore, MD 21205, USA nitish@jhu.edu

In practice, however, the curvature of rat's cortex and non-uniform laser illumination result in significant inhomogeneous impact and therefore distorted estimation of CBF and dHb images. In order to correct the non-uniform illumination, most LSI researchers [1][2][3] use lens to expand the Gaussian laser beam and then only use the central portion, which is still strictly not uniform. In this paper, we are going to model such inhomogeneity due to the curvature of cortex and non-uniform laser illumination first, and then estimate the parameters of the model with 1-D curve fitting technique to reconstruct the CBF and dHb images.

II. METHOD

A. Modeling the Inhomogeneous Impact

The inhomogeneity could be from the effects of cortex curvature and Gaussian laser illumination. The influence of cortex curvature can be approximately modeled as a part of elliptic paraboloid:

$$M_1(x,y) = a(\frac{(x-p_1)^2}{q_1^2} + \frac{(y-p_2)^2}{q_2^2}) \tag{2}$$

where (x, y) is the Cartesian coordinates, a is the scale coefficient, (p_1, p_2) is the center of elliptic paraboloid, q_1 and q_2 are the semi-axis length along x-axis and y-axis respectively. While illumination effect of Gaussian laser beam can be modeled as a 2-D Gaussian function in an ellipse.

$$M_2(x,y) = de^{-((\frac{(x-b_1)}{r_1})^2 + (\frac{(y-b_2)}{r_2})^2)} \tag{3}$$

where d is the scale coefficient, (b_1, b_2) is the center of 2-D Gaussian function, r_1 and r_2 are the semi-axis length along x-axis and y-axis respectively.

Considering the effects of both cortex curvature and Gaussian laser illumination, the overall inhomogeneity can be modeled as:

$$M(x,y) = M_1(x,y) \cdot M_2(x,y) \tag{4}$$

B. Distorted CBF and dHb Images due to Inhomogeneous Impact

According to the model Eq.(4), the distorted images of CBF and dHb, i.e. $\widetilde{I}_{CBF}(x,y)$ and $\widetilde{I}_{dHb}(x,y)$ respectively, derived from distorted raw speckle images, can be simply modeled as:

$$\widetilde{I}_{CBF}(x,y) = M(x,y) \cdot I_{CBF}(x,y) \tag{5}$$

$$\widetilde{I}_{dHb}(x,y) = M(x,y) \cdot I_{dHb}(x,y) \tag{6}$$

978-1-4244-3296-7/09/$25.00 ©2009 IEEE

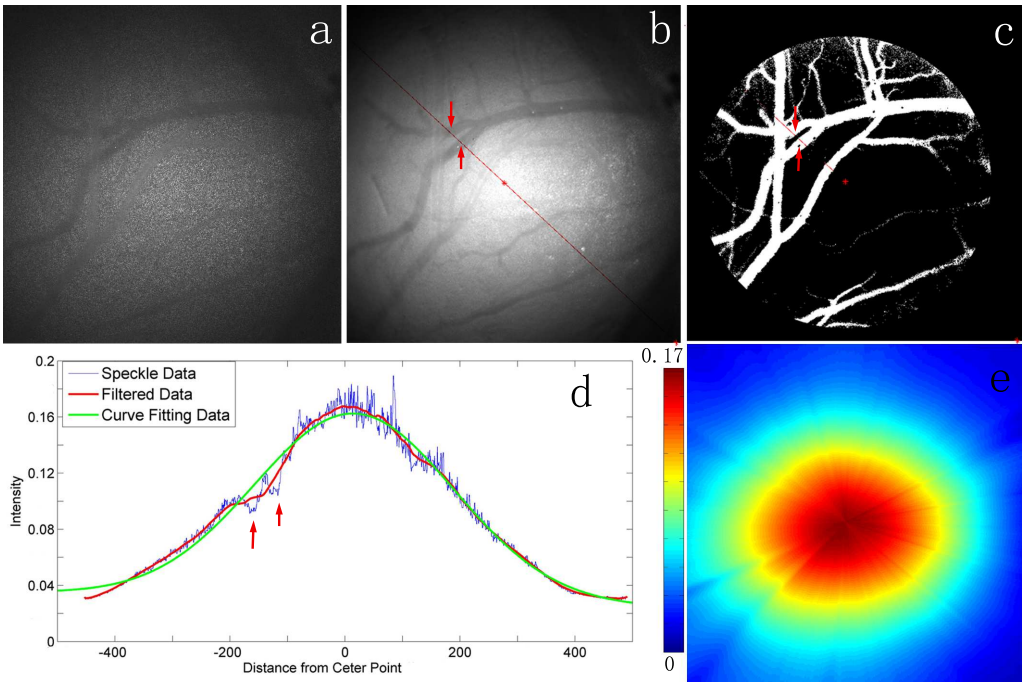

Fig. 1. Inhomogeneous Impact Model Estimation: (a) One typical image of "raw speckle images". (b) The distorted dHb image $\widetilde{I}_{dHb}(x,y)$. (c) The segmentation image. (d) The adaptive window median-mean filtering and 1-D curve fitting results of the diameter along red line in (b). Red arrows in (b,c,d) indicate two branches of venules. (e) The model estimated by our method (pseudo color is used).

where the $I_{CBF}(x,y)$ and $I_{dHb}(x,y)$ are accurate CBF and dHb images respectively.

If the inhomogeneity $M(x,y)$ can be estimated, the accurate CBF and dHb then can be reconstructed. In practice, it is very difficult to fit the complex 2-D model $M(x,y)$ based on $\widetilde{I}_{CBF}(x,y)$ or $\widetilde{I}_{dHb}(x,y)$. Furthermore, the cortex curvature is more complicated than an elliptic paraboloid. Therefore, to make a convergent estimation of $M(x,y)$ at low computing cost, 1-D curve fitting technique is used to estimate the model along each diameter of the illumination ellipse in $\widetilde{I}_{CBF}(x,y)$ instead. Accordingly, Eq.6 can be simply represented for each diameter (l):

$$\widetilde{I}_{dHb}(l) = M(l) \cdot I_{dHb}(l) \tag{7}$$

where l is the line coordinate along the ellipse diameter of laser illumination.

C. Adaptive Window Median-mean Filtering

In Eq.7, if $I_{dHb}(l)$ is approximately constant, then the model $M(l)$ can be easily estimated by 1-D curve fitting. Nevertheless, in $\widetilde{I}_{dHb}(x,y)$, the large intensity decay of the venules area makes the curve fitting inaccurate (Red arrows in Fig.1 (b, c, d)).

Therefore, in order to eliminate such intensity decay in venules and other noise, we preprocessed the $\widetilde{I}_{dHb}(l)$ with adaptive window median-mean filtering before curve fitting, i.e. the data along each diameter is smoothed firstly by the median filter with a window size $2R$ and then by the mean filter with a window size R. R is the largest vessel size across that diameter obtained by vesel segmentation (Fig.1 (c)). In this paper, we used monotonic point transform (MPT) to improve the segmentation performance [7]:

$$f_e = \int_0^f p(f)\, df \tag{8}$$

where f is the random variable for $\widetilde{I}_{dHb}(x,y)$, $p(f)$ is the probability density function of f, f_e is the output of MPT which is then segmented by Otsu multi-threshold method [8].

D. Model Estimation By 1-D Curve Fitting

The filtered data along each diameter is then used to estimate the model $M(l)$. The 1-D model $M(l)$ (Eq.9) is deduced from the 2-D model $M(x,y)$ (Eq.4). The effect of Gaussian illumination can be accordingly converted into a 1-D Gaussian function. In practice, the change of cortex curvature is relatively small, so a linear function is used to model its effect.

$$M(l) = s(l+t)e^{-(l/r)^2} \tag{9}$$

where l is the line coordinate as in Eq.7, (s,t) are the parameters of the linear function, r is the shape parameter of the Gaussian function.

Each parameter in the 1-D model (Eq.9) is estimated by 1-D curve fitting technique [9] based on the nonlinear least mean square method (Fig.1 (d)). The 2-D model $M(x,y)$ is therefore constructed (Fig.1 (e)).

E. Reconstruction

The accurate dHb (I_{dHb}) and CBF (I_{CBF}) images are reconstructed as below:

$$I_{dHb}(x,y) = \widetilde{I}_{dHb}(x,y)./M(x,y) \tag{10}$$

$$I_{CBF}(x,y) = \widetilde{I}_{CBF}(x,y)./M(x,y) \quad (11)$$

The principle of simultaneously imaging the CBF and dHb distribution by model based reconstruction is shown in Fig.2.

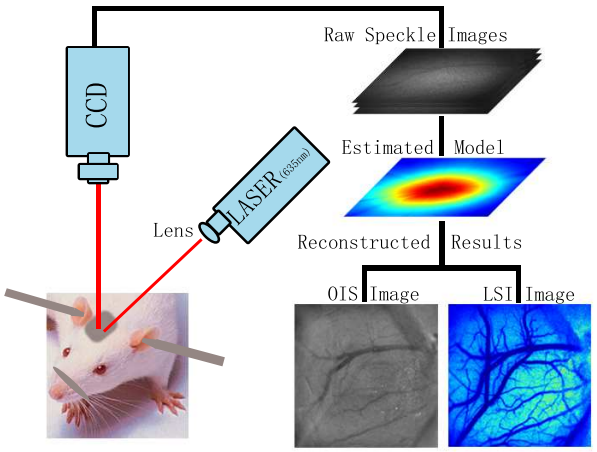

Fig. 2. The principle for simultaneously imaging the CBF and dHb by model based reconstruction.

III. EXPERIMENT AND DATA ANALYSIS

A. Animal Preparation

The animal experiment protocol used in this study is approved by the Animal Care and Use Committee of the Johns Hopkins Medical Institutions. The experimental subjects, female Sprague-Dawley rats (300g), were anesthetized with intraperitoneal (IP) injection of sodium pentobarbital (50 mg/kg). The rat was constrained in a stereotaxic frame (model 975, Kopf Instruments, Tujunga, CA). A midline incision was made over the scalp and the tissues over the bones were cleaned with a blade. A 10 by 10 mm cranial window overlying the center of right somatosensory cortex (centered of 5.5 mm lateral and 2.5-3.0 mm caudal from the bregma) was thinned with a high speed dental drill (Fine Science Tools Inc. North Vancouver, Canada) equipped with 1.4 mm steel burr until half transparent.

A 12-bit, cooled CCD camera (Sensicam SVGA, Cooke, MI) with a 60 mm macro (1:1 maximum reproduction ratio) f/2.8 lens was held by a rack and was focused on the blood vessels in the cranial window. The imaging area was illuminated with a 635 nm He-Ne Laser beam source (1805P, Uniphase, CA). The laser beam was reshaped by a lens to expand the beam range for the illumination. The resolution of image recorded by the CCD camera is 704 by 704 pixels corresponding to the imaging area of 4.7 by 4.7 mm^2. The exposure time was set to 2 ms and frame rate was 11 fps.

B. Data Processing

Sequential raw speckle images were recorded by the CCD camera in the experiment. Using the above model based reconstruction technique, we reconstruct CBF ($I_{dHb}(x,y)$) and dHb ($I_{CBF}(x,y)$) images.

TABLE I
NORMALIZED AVERAGE VALUES OF FOUR AREAS IN DISTORTED AND RECONSTRUCTED DHB IMAGES

	areaA	areaV	areaA1	areaA2
$\widetilde{I}_{dHb}$	1.0	1.12	1.78	1.45
I_{dHb}	1.0	0.854	0.993	0.994

IV. RESULTS

A. Reconstructed dHb Image

Compared with arterioles and tissue, the venules should contain more dHb [10] and thus should be relatively darker in the dHb image. The black and white circles in Fig.3 (b) indicate the large venule (LargeV) and large arteriole (LargeA) respectively.

Fig.3 (a) shows the dHb image $\widetilde{I}_{dHb}(x,y)$ directly from the OIS. The inhomogeneous impact is significant especially in the center area. Fig.3 (b) is the reconstructed dHb with elimination of the inhomogeneous impact.

Based on the vessel segmentation, four areas (black boxes in Fig.3 (c)) are selected for quantitative compare. According to the anatomy of rat's cortex, areaV covers the large venule (LargeV), areaA covers the large arteriole (LargeA), areaA1 and areaA2 are corresponding to two branches of LargeA.

Since the baseline values are different before and after reconstruction, the average value in each area is normalized by that in areaA respectively (See Table I). The dHb concentration in areaV should be higher than that in areaA. So the average intensity in areaV should be smaller than that in areaA. However, in the distorted dHb image, the average intensity in areaV (1.12) is higher than that in areaA (1.0) due to the inhomogeneity. After reconstruction with the model Eq.4, this distortion is corrected ($I_{dHb}(x,y)$)(areaV *vs* areaA is 0.854 vs 1.0).

Since areaA1 and areaA2 cover the branches of LargeA with comparable distances to the branch point, the dHb concentration was supposed to be similar with each other. So, the average intensities in areaA1 and areaA2 were suppose to be in similar level. Because of the inhomogeneous impact, central portion is brighter than the outer area, which leads the average intensity in areaA1 (1.78) higher than that in areaA2 (1.45). After the reconstruction , the average intensities in areaA1 ($I_{dHb} = 0.993$) and areaA2 ($I_{dHb} = 0.994$) are very close.

B. Reconstructed CBF Image

Fig.4 (a) shows the distorted CBF image ($\widetilde{I}_{CBF}$). The center portion is significantly affected by the inhomogeneous impact, which is clearly corrected after the reconstruction (Fig.4 (b)).

Based on the characteristics of hemodynamics in artery, along the blood flow direction, the blood velocity in the vessel is assumed constant until a bifurcation [11]. In Fig.4 (c), the centerline of one branch of LargeA is marked with red dots and the blood flow direction (yellow arrow) is also designated. There are other small bifurcations marked by red

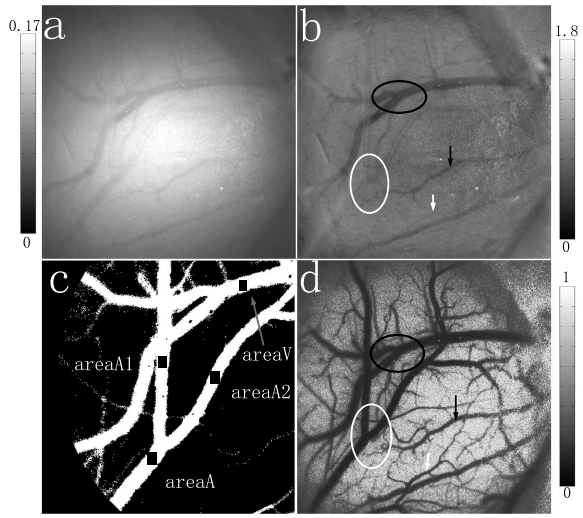

Fig. 3. Reconstruction of dHb image: (a) The distorted dHb image $\widetilde{I}_{dHb}(x,y)$. (b) The reconstructed dHb image $I_{dHb}(x,y)$. (c) Four areas (areaV, areaA, areaA1 and areaA2) are selected in the segmentation image. (d) The reconstructed CBF image $I_{CBF}(x,y)$. Combining (b) and (d), arterioles and venules can be distinguished (the black circle and arrow indicates the arterioles while the black circle and arrow show the venules.

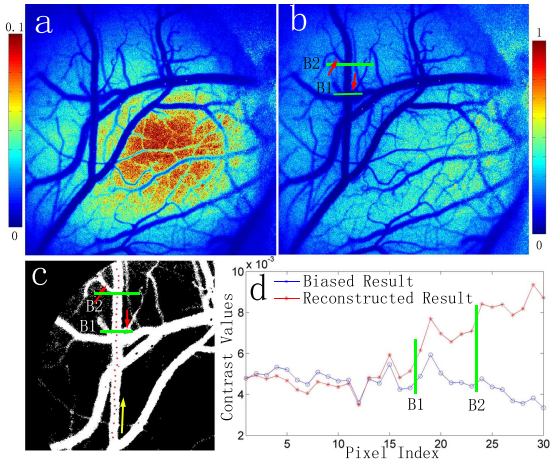

Fig. 4. Reconstruction of CBF image: (a) The distorted CBF image $\widetilde{I}_{CBF}(x,y)$. (b) The reconstructed CBF image I_{CBF}. (c) The center line (red dots) of one branch of the large arteriole are selected along the blood flow direction (yellow arrow). The red arrows in (b) and (c) show two small branches. (d) The contrast values along the blood flow direction before and after the reconstruction. The green lines (B1, B2) in (b), (c) and (d) show the interfaces of the two small branches.

arrows in Fig.4 (b, c). The CBF velocity in that branch is expected to be reducing after bifurcations (Green lines in Fig.4 (b, c)).

Accordingly, the contrast values should be kept constantly before B1, then are suppose to increase after the bifurcations at B1 and B2 sequentially. Because of the inhomogeneous impact, however, the contrast data corresponding to the CBF tended to be descending along the blood flow shown as the blue curve in Fig.4 (d)). After the reconstruction, the trend of contrast data is corrected as the expected (see the red curve in Fig.4 (d)). For the convenience of comparison, the contrast value $I_{CBF}(x,y)$ were rescaled to the same of level of $\widetilde{I}_{CBF}(x,y)$ for the first sample along the centerline in Fig.4 (d).

V. DISCUSSIONS

In the reconstructed dHb image, the venules are darker than arterioles. Therefore, combining the reconstructed CBF and dHb images, arterioles and venules can be discriminated. In Fig.3 (b,d), the black circle and arrow indicates the arterioles while the black circle and arrow show the venules.

In this paper, the trends of contrast data along the centerline of the arteriole were used for quantitative analysis which will be validated by Laser Doppler technique more accurately in the future.

VI. CONCLUSION

An automatic model based reconstruction technique is proposed for simultaneously imaging the CBF velocity and dHb distribution. Preliminary experimental results on rodent animals showed that CBF and dHb were more accurate after the reconstruction.

VII. ACKNOWLEDGMENTS

This work is supported by NIH/NIA 1R01AG029681. S. Tong is also supported by the New Century Talent Program by the Ministry of Education of China. P. Miao is also supported by the joint PhD fellowship of Shanghai Jiao Tong University and Johns Hopkins University from China Scholarship Council.

REFERENCES

[1] J. Briers and S. Webster, "Laser speckle contrast analysis (LASCA): a nonscanning, full-field technique for monitoring capillary blood flow," *J. Biomed. Opt.*, vol. 1, no. 2, pp. 174–179, 1996.

[2] A. Dunn, H. Bolay, M. Moskowitz, and D. Boas, "Dynamic Imaging of Cerebral Blood Flow Using Laser Speckle," *J. Cereb. Blood Flow Metab.*, vol. 21, pp. 195–201, 2001.

[3] W. Lau, S. Tong, and N. Thakor, "Spatiotemporal characteristics of low-frequency functional activation measured by laser speckle imaging," *IEEE Trans. Neural. Syst. Rehabil. Eng.*, vol. 13, no. 2, pp. 179–185, 2005.

[4] A. Grinvald, E. Lieke, R. Frostig, C. Gilbert, and T. Wiesel, "Functional architecture of cortex revealed by optical imaging of intrinsic signals," *Nature*, vol. 324, no. 6095, pp. 361–364, 1986.

[5] H. Cheng, Q. Luo, S. Zeng, S. Chen, J. Cen, and H. Gong, "Modified laser speckle imaging method with improved spatial resolution," *J. Biomed. Opt.*, vol. 8, no. 3, pp. 559–564, 2003.

[6] R. Frostig, E. Lieke, D. Ts'o, and A. Grinvald, "Cortical Functional Architecture and Local Coupling Between Neuronal Activity and the Microcirculation Revealed by In vivo High-Resolution Optical Imaging of Intrinsic Signals," *PNAS*, vol. 87, no. 16, pp. 6082–6086, 1990.

[7] P. Miao, M. Li, H. Fontenelle, A. Bezerianos, Y. Qiu, and S. Tong, "Imaging the Cerebral Blood Flow with Enhanced Laser Speckle Contrast Analysis (eLASCA) by Monotonic Point Transformation," *IEEE Trans. Biomed. Eng., in press*, 2009.

[8] P. Liao, T. Chen, and P. Chung, "A Fast Algorithm for Multilevel Thresholding," *J. Inf. Sci. Eng.*, vol. 17, no. 5, pp. 713–727, 2001.

[9] H. Motulsky and A. Christopoulos, *Fitting Models to Biological Data Using Linear and Nonlinear Regression: A Practical Guide to Curve Fitting*. Oxford University Press, USA, 2004.

[10] L. Edvinsson, E. MacKenzie, and J. McCulloch, *Cerebral blood flow and metabolism*. Raven Press New York, 1993.

[11] D. Ku, "Blood Flow in Arteries," *Annu. Rev. Fluid Mech.*, vol. 29, no. 1, pp. 399–434, 1997.